Unsteady forces induced by a flag in a wind tunnel

Emmanuel Virot[a], **Xavier Amandolese**[a,b], **Pascal Hémon**[a]

a. *LadHyX, CNRS UMR 7646, École Polytechnique - 91128 Palaiseau, France*

b. *Département ISME , Conservatoire National des Arts et Métiers - 75003 Paris, France*

Résumé :

Nous étudions le flottement de drapeau en soufflerie à l'aide d'une caméra rapide et d'un système de mesure d'efforts instationnaires relié à la hampe du drapeau. L'évolution de la trainée instationnaire et du moment instationnaire autour de la hampe présente différents régimes en augmentant la vitesse du vent. L'analyse des densités spectrales de puissance révèle également des changements brutaux de fréquence dominante, qui sont associés à des changements de mode de flottement. Il est notable qu'après le premier changement de mode de flottement, les densités spectrales de puissance s'étalent et les efforts sont de moins en moins périodiques.

Abstract :

We study the flag flutter in a wind tunnel by using a high-speed camera and an unsteady force measurement system connected to the flagpole. Unsteady drag force and moment around the flagpole exhibit different regimes when increasing wind velocity. Power spectral densities reveal also sudden changes of dominant frequency, which are associated to flutter mode switches. Strikingly, after the first mode switch power spectral densities spread and unsteady forces are less and less periodic.

Mots clefs : flutter, flag, wind tunnel

1 Introduction

In the early 1930s, the need to design airplanes towing advertising banners led Fairthorne to study the drag of flags and more particularly the additional drag due to flutter. In a wind tunnel, he measured drag coefficients for many textile flags and he provided empirical formulas. This seminal work led to the conclusion that the longer the flag, the smaller the drag coefficient [5]. Later, Hoerner recovered Fairthorne's data and stressed on the fact that an ordinary fluttering flag had an additional time-averaged drag force 10 times higher than the skin friction drag force [6]. Taneda confirmed this huge increase with a large range of materials [12]. Time-averaged drag force of flags was then extensively measured [9], but only few experimental studies on unsteady forces were conducted. In the present work, we provide experimental measurements of unsteady forces induced by a flag, and we highlight the link between flutter mode switches and unsteady forces acting on the flagpole.

2 Experimental techniques

A rectangular flag is cut in the 29.7 cm direction of $A4$ sheets of paper (Clairalfa 120 g/m^2). This flag has a thickness $d = 150\ \mu m$ and a mass density $\rho_p = 790\ kg/m^3$. The flag length (chord) is $L = 140\ mm$, the flag width (span) is $H = 100\ mm$ and its flexural rigidity is $\mathscr{D} = Ed^3/12(1-\nu^2) = 1.7\ mN.m$, where E is the longitudinal Young's modulus and ν is the Poisson's ratio.

The flag is placed in an Eiffel wind tunnel with a rectangular test-section : width $\times$ height $= 260\ mm \times 240\ mm$. Several views of the set-up are offered in Fig. 1. The flag is fixed inside of a flagpole of thickness 4 mm and height 140 mm. The flagpole is kept bluff in order to trigger a turbulent boundary layer all along the flag. Tests are performed for a wind velocity varying from 7.2 to 17.9 m/s, and the turbulence level - the relative importance of velocity fluctuations in the wind tunnel - is approximately 0.4% over

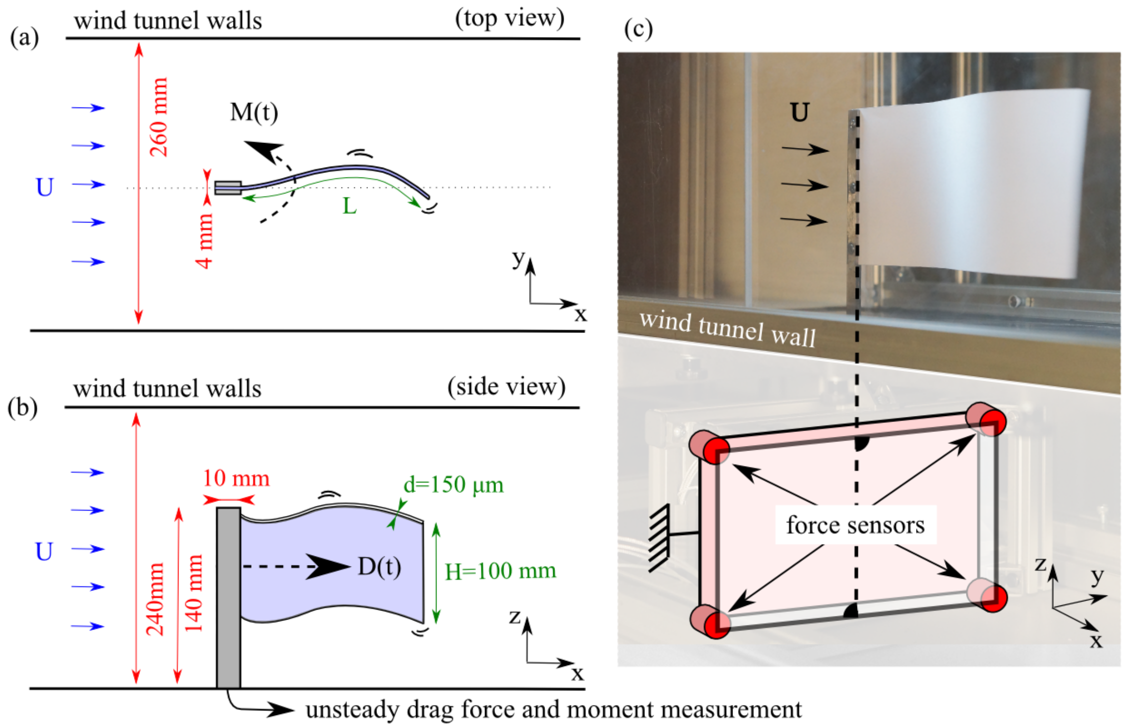

FIGURE 1 – Wind tunnel characteristics : (a) top view of the wind tunnel, containing a fluttering flag fixed on its flagpole ; (b) side view ; (c) snapshot of a fluttering flag in the wind tunnel ; the balance outside the wind tunnel is drawn : it consists in four piezoelectric force sensors connecting the flagpole with the laboratory ground.

this velocity range. Accordingly, the Reynolds number based on the flag length (L) falls in the range $Re_L = 1.4 \times 10^4 - 3.4 \times 10^5$. A high-speed video camera VDS Vosskühler HCC1000 records the flag motion from the top of the wind tunnel. It captures 462 frames per second and this is sufficient to observe approximately 20 frames per flapping period.

Our force measurement system consists in a flagpole connected to four piezoelectric force sensors Kistler 9712B5 (load cells) which record only force fluctuations (and no time-averaged value). The four force signals delivered from sensors are linearly combined to reconstruct the unsteady drag force $D(t) - < D(t) >$ and the unsteady moment around the flagpole $M(t) - < M(t) >$, where $< ... >$ refers to time-averaged value.

3 Experimental results

3.1 Dimensionless parameters

In this study we use the mass ratio M^* and the dimensionless velocity U^* defined in [3] :

$$M^* = \frac{\rho_a L}{\rho_p d}, \qquad U^* = \sqrt{\frac{\rho_p d}{\mathscr{D}}} LU \tag{1}$$

The mass ratio compares the displaced fluid mass to the displaced solid mass and the dimensionless velocity balances inertia and elasticity : this is the time-scale ratio of characteristic time of free vibration of the flag ($\sim \sqrt{\rho_p d / \mathscr{D} L^2}$) to passing time of fluid along the flag ($\sim L/U$). The studied flag has a mass ratio $M^* = 1.39$ and thus the onset of flutter is predicted to be one-neck flutter, similar to second bending mode of a cantilever beam [4].

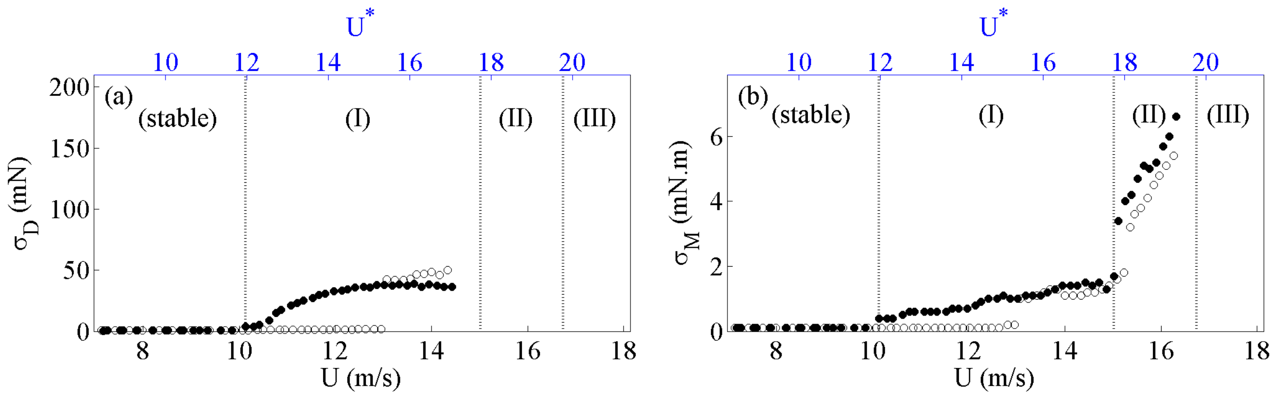

FIGURE 2 – Evolution of unsteady drag force and moment around the flagpole, characterized by their standard deviations, when increasing wind velocity ; empty circles correspond to reproducibility tests.

TABLE 1 – Wind velocities applied to the flag (see Fig. 3)

Designation	Fig. 3 (α)	Fig. 3 (β)	Fig. 3 (γ)	Fig. 3 (δ)	Fig. 3 (ϵ)	Fig. 3 (ζ)
$U\ (m/s)$ / U^*	9.2 / 10.9	11.5 / 13.6	14.9 / 17.6	15.0 / 17.7	16.9 / 20.0	17.3 / 20.4
$f\ (Hz)$	0	23	30	32	58	57

3.2 Unsteady forces measurement

Unsteady drag and moment around the flagpole are characterized by their standard deviations :

$$\sigma_D = \sqrt{< D(t)^2 > - < D(t) >^2}, \quad \sigma_M = \sqrt{< M(t)^2 > - < M(t) >^2} \tag{2}$$

Standard deviations of unsteady drag force (σ_D) and moment around the flagpole (σ_M) are presented in Fig. 2. The wind velocity is increased up to tear the flag, i.e. from 7.2 m/s to 17.9 m/s.

At $U = 10.1\ m/s$ the flag starts to flutter : in Fig. 2 we observe a sudden discontinuity followed by a gentle increase in σ_D and σ_M. There is a second strong and brutal increase in σ_M at $U = 15.0\ m/s$. A brutal increase in σ_D is also observed, but σ_D has a dominant frequency close to the cut-off frequency of our procedure (60 Hz) when $U > 15.0\ m/s$. Thus, these data are flawed and removed.

Another experiment is performed with the same flag (open circles in Fig. 2). On the one hand, we notice that the critical velocity is significantly higher for the second test. This discrepancy on the onset of flutter is attributed to the presence of a transverse curvature at the flagpole fixation.On the other hand, comparable levels of forces are obtained when the flags flutter.

3.3 Mode switches and flapping amplitude

Flutter mode switches due to an increase of wind velocity (at a given mass ratio M^*) were reported in experiments [12, 4], and predicted by numerical simulations [17, 2, 1, 10]. In practice, the fast motion of flag blurs visual observation and prevents a simple visual detection of flutter mode switches. However, we can observe them by using a high-speed camera : they are characterized by a constant number of necks. This is not surprising that each flutter mode has a given number of necks : by using the Galerkin method we can show that flutter modes correspond to specific projections on *in vacuo* cantilever beam modes [7, 8]. We can thus define regime (I), (II) and (III), the one-, two- and three-necks flutter regime observed with high-speed camera, respectively.

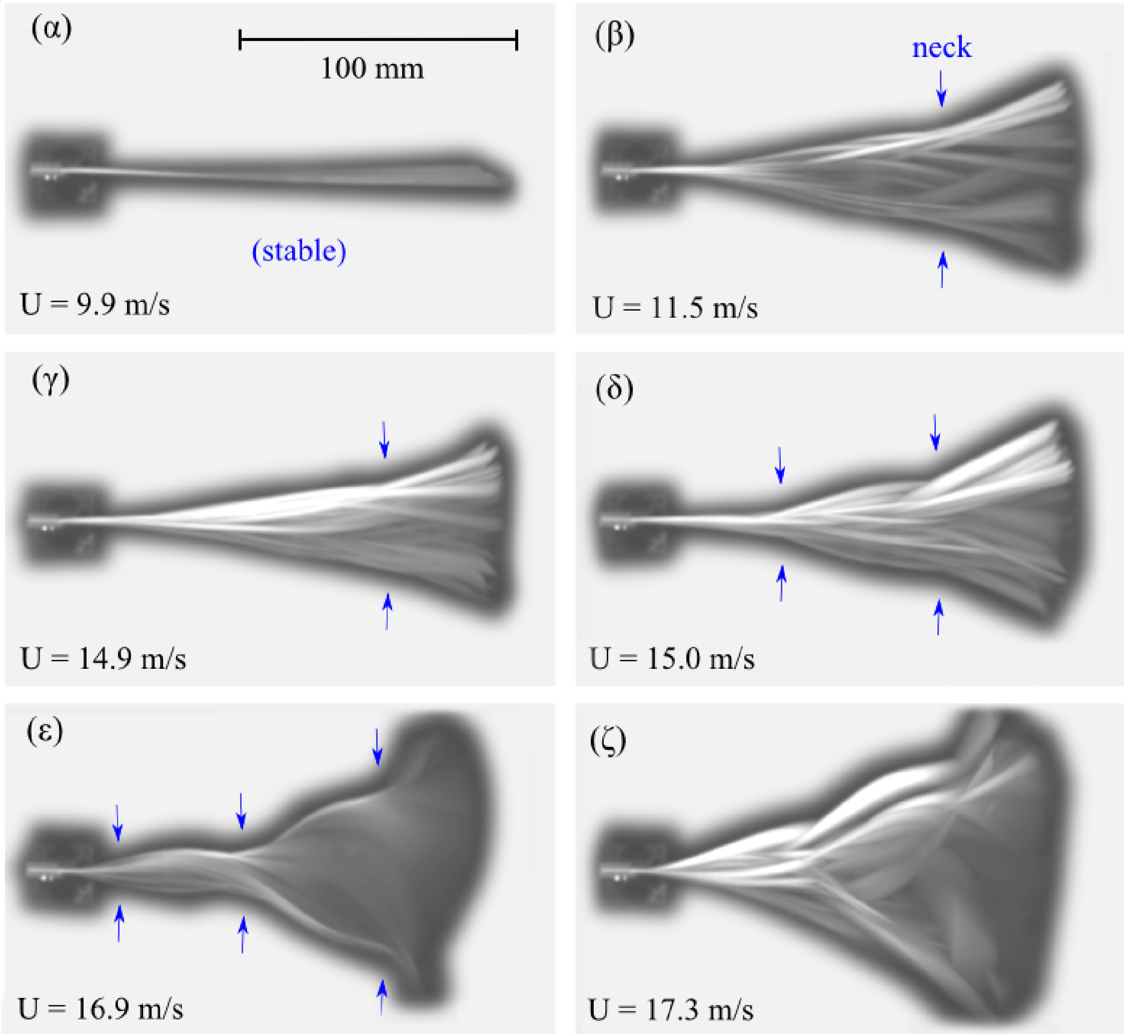

FIGURE 3 – Snapshots superimpositions of the fluttering flag at different wind velocities ; greek letters refer to table 1.

In snapshots superimpositions of Fig. 3 we can appreciate the successive flutter modes : when the wind velocity increases, one-neck flutter (Fig. 3 (δ) and Fig. 3 (γ)) is succeeded by two-necks flutter (Fig. 3 (δ)) and three-necks flutter (Fig. 3 (ϵ)). The last regime before tear is characterized by a succession of quasi-periodic and chaotic oscillations, as observed in Fig. 3 (ϵ) and Fig. 3 (ζ). The resemblance to dynamics of cylinders immersed in axial flow is striking [11].

Flapping amplitudes are reported on Fig. 4. At the onset of flutter there is an brutal increase of flapping amplitude, followed by a gentle decrease. At the transition from one-neck flutter to two-necks flutter, the amplitude is brutally increased again. In the last regime, then discrepancies reveal a loss of periodicity.

3.4 Frequency analysis

To understand better unsteady forces of Fig. 2, we studied the evolution of power spectral densities in Fig. 5. At this stage we checked successfully that the dominant frequency of moment around the flagpole was always equal to the flapping frequency measured by high-speed camera.

Firstly, we observe that the dominant frequency of unsteady drag is twice the dominant frequency of unsteady moment. Indeed, a flapping to the left and a flapping to the right influence the drag identically.

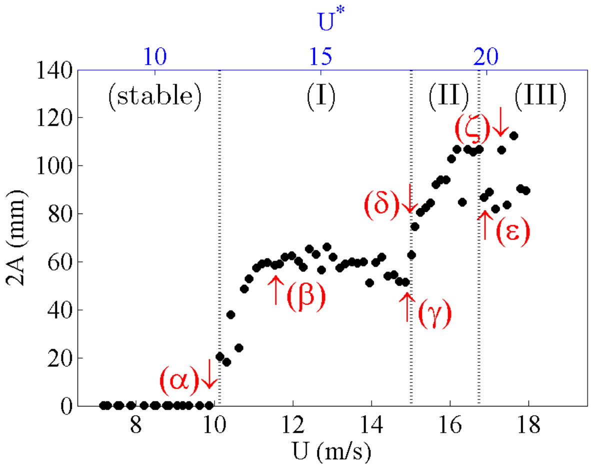

FIGURE 4 – Peak-to-peak amplitude of the flag trailing edge when increasing wind velocity : arrows (α), (β), (γ), (δ), (ϵ) and (ζ) refer to table 1 and Fig. 3.

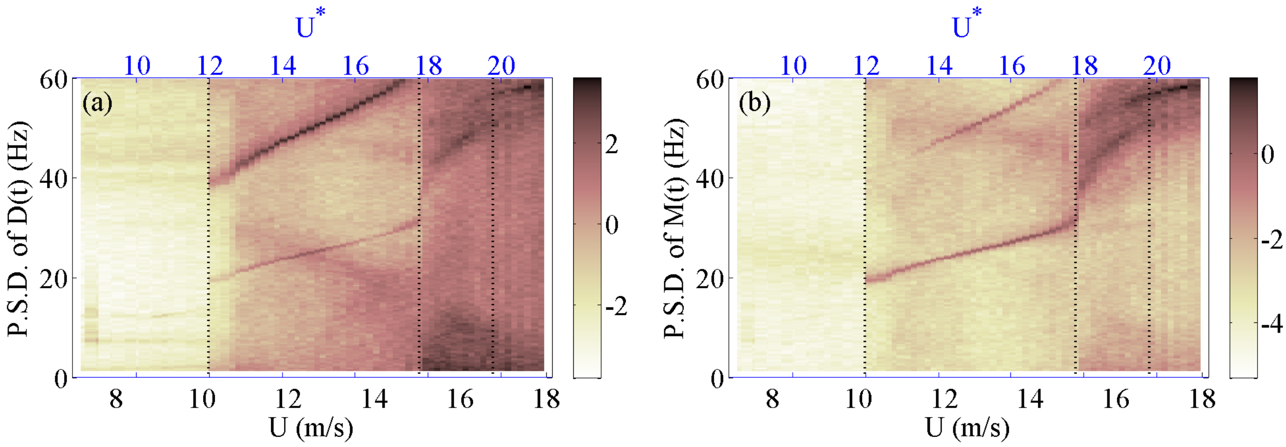

FIGURE 5 – Evolution of power spectral densities when increasing wind velocity : (a) unsteady drag force ; (b) unsteady moment around the flagpole ; color scales are logarithmic in mN^2/Hz and $mN^2.m^2/Hz$ respectively.

Secondly, we observe that dominant frequencies increase linearly with wind velocity in each flutter regime. The linearity between flapping frequency and wind velocity was evidenced long ago [12, 16] and can be justified by a local linear reasoning at fixed mass ratio [2]. Power spectral densities of Fig. 5 also exhibit upward switches of dominant frequency. When compared to theoretical works, both upward and downward stairs were predicted according to the value of mass ratio [13, 14].

By comparing Fig. 2 to Fig. 5, we observe that unsteady forces are stronger when the flapping is no longer periodic, that is to say after the first flutter mode switch at $U = 15.0\ m/s$. The loss of periodicity that we find at high wind velocity is widely predicted [17, 2, 1, 10]. This is actually common that flexible structures undergoing large excitation exacerbate chaotic properties, for instance in the context of musical instruments [15].

4 Summary and perspectives

We provided experimental measurements of unsteady drag force and unsteady moment around the flagpole, and we demonstrated that they depend strongly on flutter modes. Observed flag dynamics was expected from theoretical studies, but it was poorly studied experimentally before. After the first mode switch, we observed a loss of periodicity and a brutal increase of unsteady moment around the flagpole.

Similar studies are ongoing on longer flags since they involve higher flutter modes. We have already observed that as shorter flags, these longer flags display several mode switches which increase unsteady drag force and moment around the flagpole. A loss of periodicity at high wind velocity is also observed.

Références

[1] Alben, S., Shelley, M.J., 2008 Flapping states of a flag in an inviscid fluid : bistability and the transition to chaos. *Physical Review Letters* **100** 074301

[2] Connell, B.S.H., Yue, D.K.P., 2007 Flapping dynamics of a flag in a uniform stream. *Journal of Fluid Mechanics* **611** 97-106

[3] Eloy, C., Souilliez, C., Schouveiler, L., 2007 Flutter of a rectangular plate. *Journal of Fluids and Structures* **23** 904-919

[4] Eloy, C., Langrange, R., Souillier, C., Schouveiler, L., 2008 Aeroelastic instability of cantilevered flexible plates in uniform flow. *Journal of Fluid Mechanics* **248** 513-520

[5] Fairthorne, R.A., 1930 Drag of flags. *Aeronautical Research Committee, Reports and Memoranda.* **1345** 887-891

[6] Hoerner, S.F., 1993 Fluid dynamic drags. 3.25

[7] Howell, R.M., Lucey, A.D., Carpenter, P.W., Pitman, M.W., 2009 Interaction between a cantilevered-free flexible plate and ideal flow. *Journal of Fluid and Structures* **25** 544-566

[8] Huang, L., Zhang, C., 2013 Mode analysis of cantilever plate flutter. *Journal of Fluid ans Structures* **38** 273-289

[9] Martin, A., 2006 Experimental study of drag from a fluttering flag. *Oklahoma State University, Master thesis* 1-136

[10] Michelin, S., Llewellyn Smith, S.G., Glover, B.J., 1993 Vortex shedding model of a flapping flag. *Journal of Fluid Mechanics* **617** 1-10

[11] Paidoussis, M.P., 1966 Dynamics of flexible slender cylinders in axial flow. Part 2. Experiments. *Journal of Fluid Mechanics* **26(4)** 737-751

[12] Taneda, S., 1968 Scaling laws for fully developed turbulent shear flows. Part 1. Basic hypotheses and analysis. *Journal of the Physical Society of Japan.* **24(2)** 392-401

[13] Tang, D.M., Yamamoto, H., Dowell, E.H., 2003 Flutter and limit cycle oscillations of two-dimensional panels in three-dimensional axial flow. *Journal of Fluids and Structures* **17** 225-242

[14] Tang, L., Paidoussis, M.P., 2007 On the instability and the post-critical behaviour of two-dimensional cantilevered flexible plates in axial flow. *Journal of Sound and Vibration* **305** 97-115

[15] Touze, C., Bilbao, S., Longo-Mucciante, L., Cadot, O., Boudaoud, A., 2010 Vibrations chaotiques de plaques minces : application aux instruments de type cymbale. *10ème Congrès Francais d'Acoustique*

[16] Uno, M., 1973 Fluttering of flexible bodies. *Journal of the Textile Machinery Society of Japan* **26(8)** 73-79

[17] Yadykin, Y., Tenetov, V., Levin, D., 2001 The flow-induced vibration of a flexible strip hanging vertically in a parallel flow. Part 1 : Temporal aeroelastic instability. *Journal of Fluids and Structures* **15** 1167-1185